Miner Deposita (2008) 43:111–124
DOI 10.1007/s00126-007-0160-4

ARTICLE

Geochronology and stable isotope signature of alteration related to hydrothermal magnetite ores in Central Anatolia, Turkey

Robert Marschik · Richard Spikings · Ilkay Kuşcu

Received: 8 February 2007 / Accepted: 12 July 2007 / Published online: 17 August 2007

Abstract Hydrothermal iron ores at Divriği, east Central Anatolia, are contained in two orebodies, the magnetite-rich A-kafa and the limonitic B-kafa (resources of 133.8 Mt with 56% Fe and 0.5% Cu). The magnetite ores are hosted in serpentinites of the Divriği ophiolite at the contact with plutons of the Murmano complex. Hydrothermal biotite from the Divriği A-kafa yield identical weighted mean plateau ages of 73.75±0.62 and 74.34±0.83 Ma (2σ). This biotite represents a late alteration phase, and its age is a minimum age for the magnetite ore. Similar magnetite ores occur at Hasançelebi and Karakuz, south of Divriği. There, the iron ores are hosted in volcanic or subvolcanic rocks, respectively, and are associated with a voluminous scapolite ± amphibole ± biotite alteration. At Hasançelebi, biotite is intergrown with parts of the magnetite, and both minerals formed coevally. The weighted mean plateau ages of hydrothermal biotite of 73.43±0.41 and 74.92±0.39 Ma (2σ), therefore, represent mineralization ages. Hydrothermal biotite from a vein cutting the scapolitized host rocks south of the Hasançelebi prospect has a weighted mean plateau age of 73.12±0.75 Ma (2σ). This age, together with the two biotite ages from the Hasançelebi ores, constrains the minimum age of the volcanic host rocks, syenitic porphyry dikes therein, and the scapolite alteration affecting both rock types. Pyrite and calcite also represent late hydrothermal stages in all of these magnetite deposits. The sulfur isotope composition of pyrite between 11.5 and 17.4‰ $\delta^{34}S_{(VCDT)}$ points towards a non-magmatic sulfur source of probably evaporitic origin. Calcite from the Divriği deposit has $\delta^{18}O_{(VSMOV)}$ values between +15.1 and +26.5‰ and $\delta^{13}C_{(VPDB)}$ values between −2.5 and +2.0‰, which are compatible with an involvement of modified marine evaporitic fluids during the late hydrothermal stages, assuming calcite formation temperatures of about 300°C. The presence of evaporite-derived brines also during the early stages is corroborated by the pre-magnetite scapolite alteration at Divriği, and Hasançelebi-Karakuz, and with paleogeographic and paleoclimatic reconstructions. The data are compatible with a previously proposed genetic model for the Divriği deposit in which hydrothermal fluids leach and redistribute iron from ophiolitic rocks concomitant with the cooling of the nearby plutons.

Keywords Divriği · Karakuz · Hasançelebi · Hydrothermal magnetite ores

Editorial handling: B. Lehmann

R. Marschik (✉)
Department of Earth and Enviromental Sciences,
Ludwig-Maximilians Universität,
Luisenstrasse 37,
80333 Munich, Germany
e-mail: marschik@lmu.de

R. Spikings
Department of Mineralogy, Université de Genève,
13, Rue des Maraîchers,
1205 Geneva, Switzerland

I. Kuşcu
Department of Geology, Muğla Üniversitesi,
48100 Kötekli-Muğla, Turkey

Introduction

The iron and steel industry of Turkey is growing fast. The steel production in 2005 was 20.9 Mt, i.e., 2% of the total world production (USGS 2007). Most of the Turkish iron ore comes from central Eastern Anatolia, and the iron deposits in the Sivas–Malatya region account for about 61% of the country's production. Divriği, Dumluca, Bizmişen, Çetin-

kaya, Otlukilise (Sivas) and Deveci, Karakuz, and Sivritepe (Malatya) are the most important operating mines in this region (Table 1). The Divriği (e.g., Klemm 1960), Karakuz (Uçurum et al. 1996), and Hasançelebi (e.g., Stendal et al. 1995) deposits in the Hekimhan area are the subjects of this work (Fig. 1). The origin of these geologically similar iron deposits is controversial. Klemm (1960) and Isik (2005) proposed a contact metasomatic (skarn) origin for Divriği. In contrast, Stendal and Ünlü (1991) and Ünlü et al. (1995) suggest that the Divriği iron ore is genetically linked with the serpentinization process of ophiolitic rocks and that the high-grade ore is formed as a result of leaching and redistribution of the iron by later hydrothermal events related to pluton emplacement. Uçurum et al. (1996) favor an orthomagmatic genetic model for the iron ores at Karakuz. Similarities of these Anatolian iron deposits with those of the iron oxide (Cu–U–Au–REE) class (e.g., Williams et al. 2005) have also been proposed (e.g., Kuşcu et al. 2002, 2005a; Yılmazer et al. 2003; Ay et al. 2004; Yigit 2006). In this contribution, we present new geochronological and isotope geochemical data and discuss their implication for the iron mineralization and the evolution of the host rocks.

Geologic context

The region between Sivas and Malatya in eastern Central Anatolia is essentially a tectonic collage of obducted slices of oceanic crust and marine limestones, which are intruded by postcollisional, silica oversaturated, alkaline, syenite–monzonite and monzogabbro-monzodiorite plutons (e.g., Dumluca, Murmano, or Hasançelebi plutons; Boztuğ 1998). These rocks are overlain by an Eocene to Pliocene–Pleistocene cover sequence. The area belongs to the Tauride tectonic unit, which is linked to the formation of the Neo-Tethyan ocean during the Early Jurassic and its closure during the Late Cretaceous (e.g., Şengör and Yılmaz 1981; Robertson 2002; Parlak et al. 2006).

Table 1 Reserve figures of selected iron deposits in the Sivas–Malatya region (DPT 2001; Anonymous 2003)

Mine	Proven	Probable	Total	(% Fe)
Divriği A-kafa	41,000	–	41,000	54
Divriği B-kafa	10,000	–	10,000	56
Dumluca	200	–	200	57
Purunsur	100	1,800	1,900	55
Taşlıktepe	60	300	360	62
Otlukilise	1,420	1,000	2,420	54
Çetinkaya	3,500	–	3,500	54
Karakuz	–	–	14,500[a]	40–55
Ekinbaşı	9,700	2,300	12,000	55
Deveci	48,000	–	48,000	38

Reserves in 1,000 tonnes
[a] Proven and probable combined

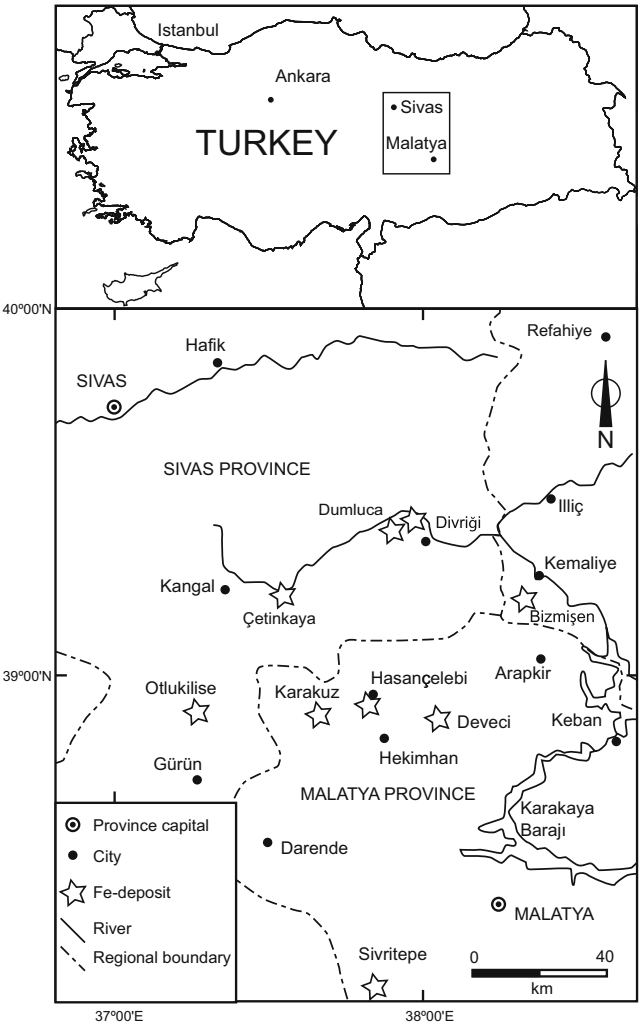

Fig. 1 Location map of the Sivas–Malatya region

The Munzur Limestone represents the lowermost unit in the Divriği area (Fig. 2) and has a thickness of approximately 1,200 m (Tunc et al. 1991). The fossil content indicates Early Carboniferous to Campanian ages (Ötztürk and Öztunali 1993; Yılmaz et al. 2001). The Munzur Limestone is tectonically overlain by the Yeşiltaşyayla ophiolitic mélange. The mélange, in turn, is either tectonically overlain by metamorphic sole rocks that are related to ophiolite obduction, serpentinites, or it is covered by Tertiary sediments, depending on the location (e.g., Parlak et al. 2006). The Divriği ophiolite represents a fairly complete section through the upper part of the oceanic crust. It consists of serpentinized mantle tectonite, layered cumulate and isotropic gabbro, and sheeted dikes (Parlak et al. 2006). According to Parlak et al. (2006), the Divriği ophiolite formed in a supra-subduction zone tectonic setting that developed in the Late Cretaceous in the Inner Tauride

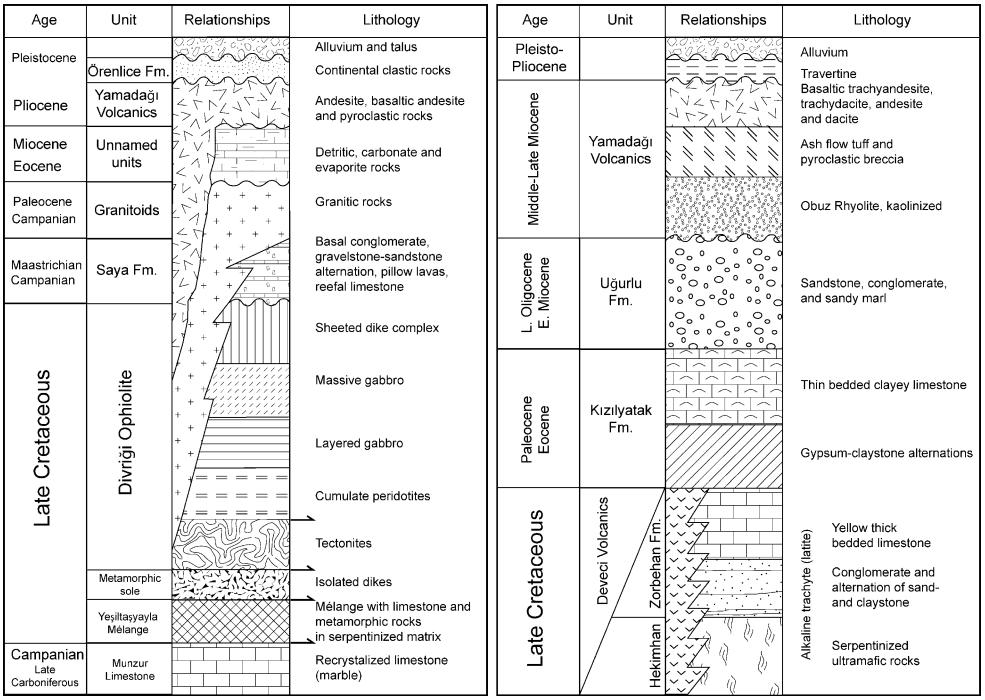

Fig. 2 Schematic stratigraphic sections of the Divriği (*left*) and Hekimhan (*right*) areas (after Parlak et al. 2006 and Yalçin et al. 1998)

ocean area, which was situtated between the Kirsehir block to the north and the Tauride platform to the south. Volcano-sedimentary rocks of the Saya Formation unconformably overlie the Divriği ophiolite. This unit contains conglomerates with ophiolite-derived pebbles at the base, which pass into an alternation of sand-, mudstone and marl, agglomerate, tuff, and altered volcanic rocks. This sequence is intruded by mafic dikes. Fossils in limestone lenses yield Campanian–Maastrichian ages (Yılmaz et al. 2001).

Alkaline granitoid plutons of mostly monzonite to syenite or monzogabbro to monzodiorite compositions intruded the Cretaceous ophiolitic suture zone mainly between Campanian (Late Cretaceous) and Danian (early Paleocene; e.g., Boztuğ and Harlavan 2007). The generation of these magmas is discussed in controversy. The magmas have been linked, e.g., to the slab break-off stage of the Neo-Tethyan convergence system along the Izmir–Ankara–Erzincan suture zone (e.g., Boztuğ and Harlavan 2007) or related to extension driven by slab roll-back, which caused invasion of hot asthenosphere (Kuşcu et al. 2007).

Most of the rocks of the Dumluca and Murmano plutonic complexes are metaluminous, showing high-K characteristics, though highly differentiated members of the felsic rocks are peraluminous in character (Boztuğ et al. 2007). Kuşcu et al. (2005a) pointed out that the alkaline composition of the granitoids at Divriği could be related to alkaline metasomatism associated with the Fe mineralization in the area. Average $\delta^{18}O$ values for the felsic rocks of the Dumluca and Murmano pluton complexes are 10.5 or 11.7‰, respectively, whereas mafic members have average values of 8.3 or 9.6‰, respectively (Boztuğ et al. 2007). Analogue, $\delta^{34}S$ values in the felsic rocks average 4.7 or 15.7‰ and those in the mafic rocks 2.4 or 7.4‰, respectively. Based on stable and some radiogenic isotope data, Boztuğ et al. (2007) conclude that the magmas contain a significant crustal component and that the Murmano suite incorporated significantly more crustal material during ascent than the Dumluca suite. They also suggest that sulfur in these magmas is derived from assimilated evaporitic components. Zeck and Ünlü (1988) report a whole rock Rb–Sr isochron age of 110±5 Ma (1σ) for the Murmano pluton. K–Ar geochronology of magmatic hornblende and/or biotite yield cooling ages ranging from 76.6±0.6 to 77.2±1.8 Ma (1σ) for the felsic, and from 62.1±0.3 to 77.4±1.5 Ma (1σ) for mafic rocks of the Murmano plutonic complex (Boztuğ et al. 2007). Hornblende or biotite K–Ar ages for the felsic rocks of the Dumluca complex range from 71.5±0.1 to 75.6±0.1 Ma (1σ) and, for the mafic rocks, from 67.8±0.4 to 76.6±1.6 Ma (1σ). Boztuğ et al. (2007) suggest that the cooling of the felsic and mafic rocks of the Murmano and Dumluca complexes below the closure temperatures of Ar retention of hornblende (450–550°C) and biotite (~300 to 350°C, e.g., McDougall and Harrison 1988) occurred at about 77 to 68 Ma and that the younger ages are reset due to Ar loss. The plutons, in turn, are intruded by numerous aplite and intermediate (diabase) dikes (Parlak et al. 2006). The cover sequence around Divriği is of Eocene to Pliocene–Pleistocene age and consists of epiclastic conglomerates, carbonate rocks, evaporites, and volcanic rocks. An Eocene basal conglomerate with pebbles

of granitoid rocks and ophiolitic rocks, and with iron ore clasts unconformably overlies the granitoids near Divriği (Parlak et al. 2006).

In the Hekimhan area, the Upper Cretaceous Hekimhan ophiolitic mélange represents the base of the stratigraphic section (Figs. 2 and 3). It consists primarily of gabbro, wehrlite, and pyroxenite, which are serpentinized in thrust and fault zones (Stendal et al. 1995). The ophiolitic rocks are overlain by a sedimentary sequence consisting of a basal conglomerate, sandstones, shales, and limestones (Zorbehan Formation). Both the ophiolitic and the sedimentary rocks have an unconformable upper contact with an Upper Cretaceous volcano-sedimentary unit that is cut by numerous syenite porphyry, microsyenite, and mafic dikes (Stendal et al. 1995). The volcano-sedimentary unit includes altered trachyte (latite) and trachyandesitic volcanic rocks (Deveci Volcanics; Yılmaz et al. 1993; Fig. 2). The trachytic rocks, for which K–Ar ages of 76 to 71 Ma have been reported (Leo et al. 1973 in Stendal et al. 1995), are assumed to be genetically related to Upper Cretaceous to Paleocene syenitic intrusive rocks (e.g., Hasançelebi pluton; Gürer 1996).

The ophiolite obduction in the region was completed before Maastrichtian times, and plutons have been emplaced after thrusting (e.g., Ilbeyli et al. 2004). Segmentation of the region into subbasins with high evaporation rates can be assumed (see, e.g., Gürer 1994; Yılmaz and Yılmaz 2006). Fossil nanoplankton abundance in the Hekimhan Formation and stable isotope data suggest that the climate in Early Campanian–Early Maastrichtian interval was probably tropical to subtropical (Yildiz and Özdemir 1999). The calculated sea-surface water temperatures are around 28.5°C and were stable through the Campanian–Early Maastrichtian. Deposition of gypsum, shale, and shaly limestone (Kızılyatak Formation) followed in the Paleocene–Eocene. The Oligocene is represented by the Uğurlu Formation, which is composed of shale, marl, sandstone, and conglomerate with limestone and coal lenses. This unit is overlain by the Middle–Upper Miocene Yamadağı Volcanics, which consists of volcanic rocks of basaltic andesite, dacitic, and rhyolite composition (Yalçin et al. 1998).

Iron deposits

Divriği deposit

The most important iron mine in the Sivas–Malatya region, which is currently in production, is located north of the city of Divriği (long. 38°04′26″ E; lat. 39°25′36″ N; Fig. 1). The Divriği mine (resources of 133.8 Mt with 56% Fe and 0.5% Cu; Yigit 2006) extracts ores from two orebodies, the A-kafa and the B-kafa (Figs. 4 and 5). A third body, the C-kafa, is an associated uneconomic placer deposit (Yigit 2006). The A-kafa ore mainly consists of massive magnetite with up to 5% disseminated pyrite, and traces of pyrrhotite, and chalcopyrite (Helke 1955; Ünlü et al. 1995). It is located along the contact between a syenite–monzonite and a monzonite porphyry of the Murmano plutonic complex to the north, with serpentinites containing large listwanite veins to the south (Fig. 5). Brecciated recrystallized limestones to the southwest contain B-kafa ore, which consists of maghemitized or martitized magnetite and

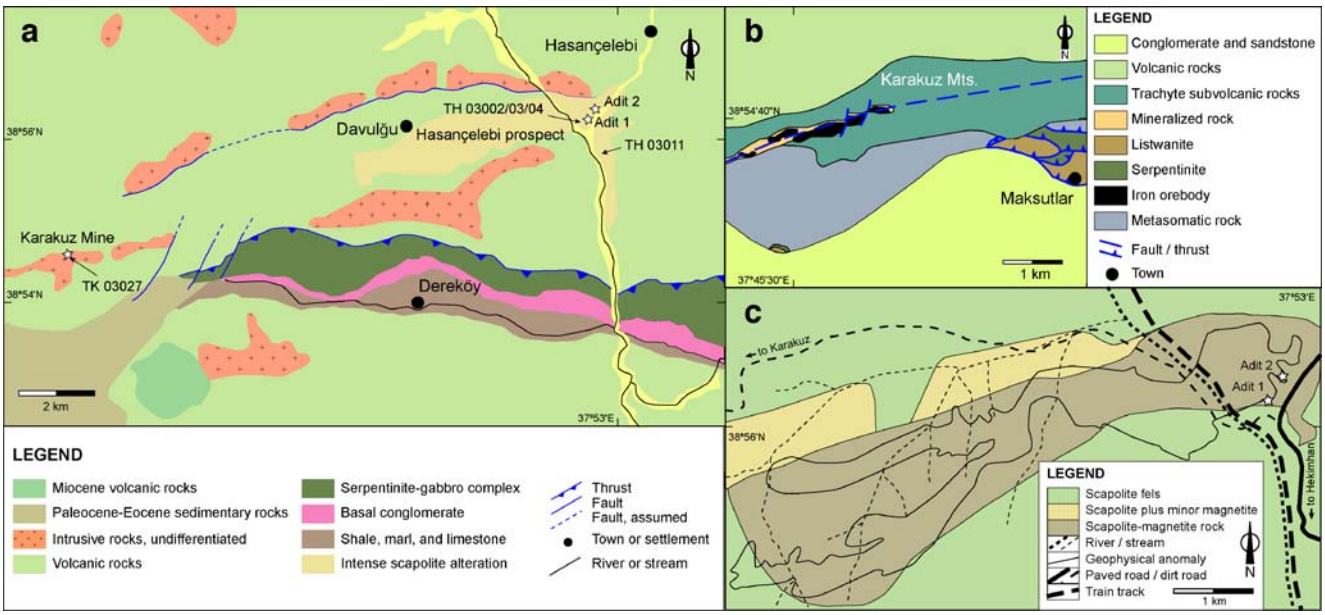

Fig. 3 **a** Geological map of the Hasançelebi-Karakuz area (after Stendal et al. 1995); **b** geology in the Karakuz mine area (after Uçurum et al. 1996); **c** alteration map of the Hasançelebi prospect (after Özkoçak 1970)

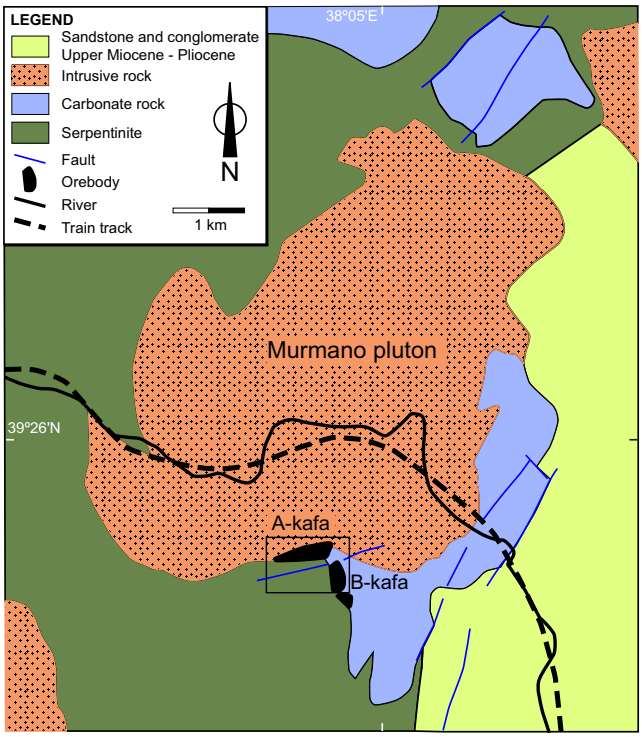

Fig. 4 Simplified geological map of the Divriği mine area (after Zeck and Ünlü 1991). The *square* indicates the position of the map of Fig. 5

limonite, plus minor sulfides (e.g., Ünlü et al. 1995; Yılmazer et al. 2003), and which are regarded as late-stage alteration products (Kuşcu et al. 2002).

Kuşcu et al. (2002) and Yılmazer et al. (2003) recognize an early scapolitization and a later retrograde stage of potassium metasomatism. The A-kafa magnetite ore is spatially associated with secondary K-feldspar and biotite (Fig. 5). Green hydrothermal biotite occurs in continuous and discontinuous veinlets and is dispersed within the massive magnetite (Fig. 6a). Pyrite and calcite belong to the latest hydrothermal alteration stage. The pyrite may or may not be spatially associated with green biotite and/or calcite in the A-kafa ore. The syenite–monzonite and monzonite porphyry are intensely altered. Fracture-controlled silicate alteration includes scapolite, andraditic garnet, pyroxene, amphibole, biotite, and tourmaline. These are cut locally by late calcite veinlets. Multiple utilization of fractures by the hydrothermal fluid(s) resulted in complex vein associations. Magnetite ± pyrite occurring in the center of previously formed veins and veinlets are common. Pyrite is also disseminated within the igneous rocks.

Karakuz and Hasançelebi iron ores

The iron ores of Karakuz and Hasançelebi are hosted intensely metasomatised, scapolite-rich Upper Cretaceous trachytic–trachyandesitic subvolcanic (Uçurum et al. 1996) or volcanic and volcaniclastic rocks, respectively (Deveci Volcanics; Fig. 3). At Karakuz (long. 37°46′00″ E; lat. 38°54′42″ N), five iron ore lenses occur along a northeast-to-southwest trending, 50-to-60° southward dipping structure (Fig. 3). Reported reserves are 14.5 Mt at 40 to 55% Fe (Anonymous 2003). The thicknesses of the ore lenses vary between 3 and 10 m. The ores mainly consist of magnetite and hematite, although goethite, lepidocrocite, and limonite are also present (Uçurum et al. 1996). Martitization is common (Uçurum et al. 1996), and mushketovitization, the replacement of early plated hematite by magnetite, has been observed (Fig. 6b). The ores at Karakuz have low phospho-

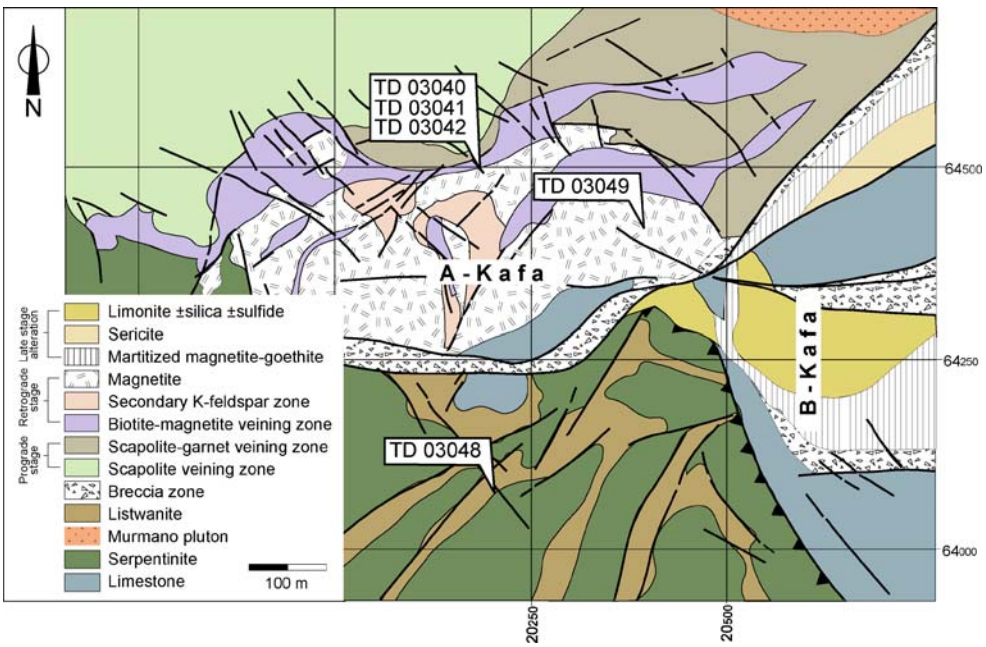

Fig. 5 Distribution of major lithologic units, ore, and alteration assemblages in the Divriği mine area (after Yılmazer et al. 2003)

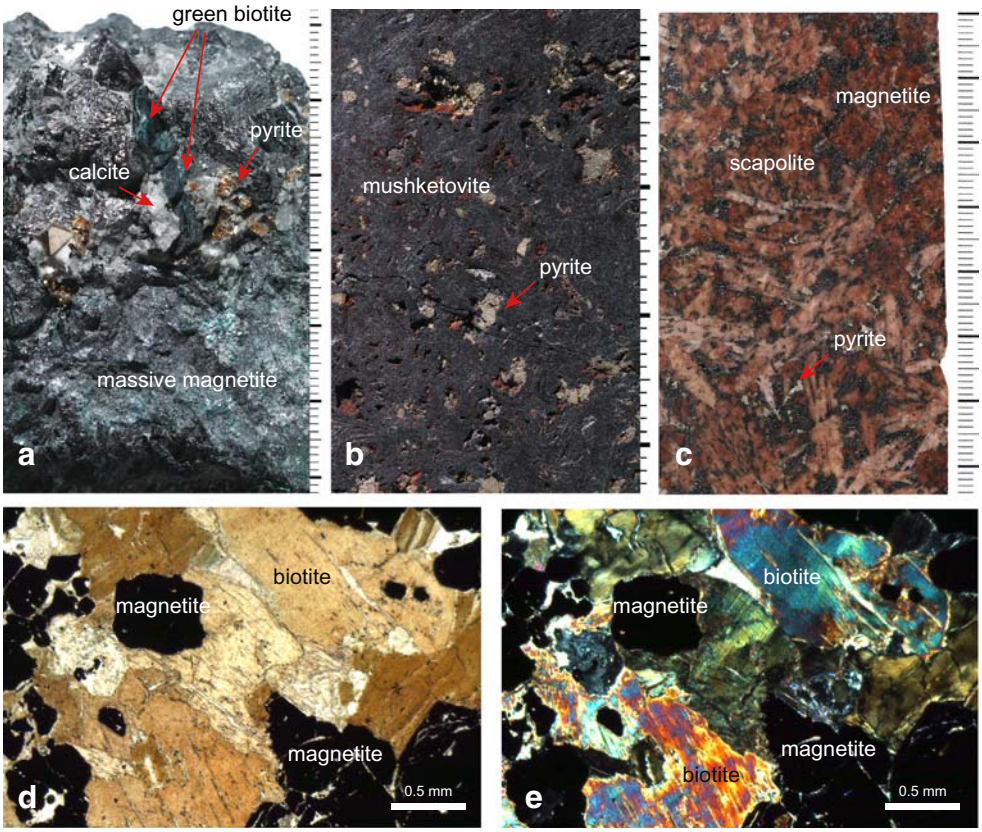

Fig. 6 **a** Handspecimen of massive magnetite with pyrite and green hydrothermal biotite from the Divriği A-kafa (attached *scale bars* in centimeters); **b** drill core samples from hole HS-2 at Karakuz showing the replacement of specular hematite by magnetite (mushketovite) with interstitial pyrite; **c** scapolite with interstitial magnetite is typically observed around the orebodies of Karakuz and Hasançelebi; **d** and **e** photomicrograph of brown hydrothermal biotite intergrown with magnetite from the Hasançelebi prospect (parallel and crossed Nicols)

rus contents (Uçurum et al. 1996). Main gangue minerals are quartz, calcite, and barite (Uçurum et al. 1996). The predominant alteration type surrounding the deposits apart from the voluminous scapolite alteration is kaolinitization.

The Bizim orebody, which is approximately 10 m wide and 150 m long, is currently in production. Its vertical dimension is known from drilling to a depth of 100 m. The Bizim ore consists mainly of massive magnetite–hematite and locally minor pyrite. The average grade is 57 to 58% Fe, although it may reach as high as 62%. The massive magnetite–hematite lens has a tectonic hanging wall contact. The hanging wall rocks are replaced by scapolite with interstitial magnetite (see Fig. 6c). Locally, stockwork or patchy hematite–magnetite or quartz–magnetite veinlets cut these scapolite-rich rocks. The Sifir orebody is already mined out. It contained stockwork-type hematite plus limonite ore with minor pyrite and high grade zones, which reached 58% Fe.

Exploration activities have identified significant iron ores in the Hasançelebi area (long. 37°52′41″ E; lat. 38°56′17″ N), north of Hekimhan, roughly along strike of the structure that controls the Karakuz orebodies (Fig. 3). The Hasançelebi district contains resources of 685 Mt with 19% Fe and locally up to 0.8% Cu and 2 g/t Au (Cihnioğlu et al. 1994; Ay et al. 2004). The iron ores occur in a 6-km-long and 0.3-km-wide area (Fig. 3; Stendal et al. 1995; Gumus 1998). The mineralization is thought to be related to the surrounding scapolite ± pyroxene ± amphibole ± biotite alteration (Kuşcu et al. 2005b), which has also affected parts of the Hasançelebi pluton (Yılmaz et al. 1993). Magnetite occurs interstitial to scapolite (Fig. 6c), and is intergrown with amphibole and/or biotite. Calcite is a late alteration phase, and calcite veinlets and microveinlets cut magnetite, amphibole, and biotite. Paragenetic relationships and the succession of alteration and mineralization phases are very similar to those at Divriği. Early scapolitization is followed by magnetite, retrograde potassium metasomatism with biotite and K-feldspar, and sericitization. Calcite and sulfides were introduced during the later alteration stages (Ay et al. 2004).

Geochronology

Sampling

Coarse-grained (0.3 to 1 cm) biotite, targeted for $^{40}Ar/^{39}Ar$ analyses, was hand-picked from both outcrops and hand-specimens. Two samples of green hydrothermal biotite from the Divriği A-kafa deposit (TD 03040 and TD 03041) have been analyzed (Table 2). The green biotite is paragenetically later than the massive magnetite and is spatially associated with pyrite and calcite (Fig. 6a).

The biotites from the Hasançelebi prospect were extracted from two magnetite-rich samples (TH 03002 and

Table 2 Samples used in this study

Sample	Location	Provenance	Description	Analyses
TH 03002	Hasançelebi	Adit 1, Fig. 3	Amphibole-rich rock with magnetite–biotite–calcite plus minor pyrite	Geochronology
TH 03003	Hasançelebi	Adit 1, Fig. 3	Magnetite-rich breccia with biotite and late calcite–pyrite	Geochronology
TH 03004	Hasançelebi	Adit 1, Fig. 3	Magnetite-K-feldspar-rich rock with biotite, calcite, and minor pyrite	S-isotopes
TH 03011	Hasançelebi	Road Hasancelebi-Hekimhan, Fig. 3	Vein of biotite cutting scapolitized Deveci Volanics	Geochronology
TK 03027	Karakuz	Drill core HS-2, Fig. 3	Massive musketovite with interstitial pyrite	S-isotopes
TD 03033	Divriği	A-kafa	Calcite vein with 2 generations of calcite plus pyrite, toumaline	C–O–S-isotopes
TD 03035	Divriği	A-kafa	Postmagnetite calcite veinlet cut by pyrite	C–O-isotopes
TD 03040	Divriği	A-kafa, Fig. 5	Magnetite with biotite, disseminated pyrite, and calcite	Geochronology, S-isotopes
TD 03041	Divriği	A-kafa, Fig. 5	Massive magnetite with biotite, pyrite and calcite	Geochronology
TD 03042	Divriği	A-kafa, Fig. 5	Massive magnetite with pyrite and calcite	S-isotopes
TD 03044	Divriği	Murmano pluton, northern pit face	Barren calcite veinlet cutting intrusive rocks	C–O-isotopes
TD 03048	Divriği	Ophiolite, southern pit face, Fig. 5	Calcite veinlet in serpentinite	C-O-isotopes
TD 03049	Divriği	A-kafa, Fig. 5	Postmagnetite calcite and pyrite veins	C-O-S-isotopes

TH 03003) that were collected from dumped material from an exploration drift. Brown and green biotite both occur in the Hasançelebi prospect. Brown biotite grains targeted for $^{40}Ar/^{39}Ar$ analyses were extracted from samples where they are spatially associated with calcite (TH 03002) or occur as flakes within calcite (TH 03003; Table 2). Another sample of brown biotite (TH 03011) was taken from a road cut (long. 37°52′51″ E; lat. 38°55′51.9″ N) along the road from Hekimhan to the Hasançelebi prospect and forms part of a biotite vein that is several centimeters wide and is hosted within a structural disrupted zone that cuts scapolite-rich rocks of the Deveci Volcanics (Table 2).

Analytical method and results

Isotopic dating was carried out at the $^{40}Ar/^{39}Ar$ laboratory of the Department of Mineralogy, University of Geneva, Switzerland. The samples were measured with an Argus (GV Instruments) multicollector mass spectrometer, equipped with four high-gain (10E12 Ohms) Faraday collectors for the analysis of ^{39}Ar, ^{38}Ar, ^{37}Ar, and ^{36}Ar, as well as a single Faraday collector (10E11 Ohms) for the analysis of ^{40}Ar. The automated UHV stainless steel gas extraction line incorporates one SAES AP10 getter and one water-cooled SAES GP50-ST707 getter. Single grains of biotite (≤0.5 cm across) were step-heated using a defocused 30-W, MIR10 IR (CO_2) laser that was rastered over the samples to provide even-heating of the grains. Samples were measured on the Faraday collectors and time-zero regressions were fitted to data collected from 12 cycles. Peak heights and blanks were corrected for mass discrimination, isotopic decay of ^{39}Ar and ^{37}Ar and interfering nucleogenic Ca-, K-, and Cl-derived isotopes. The high stability of the Faraday baseline measurements (varation is <0.1% over periods of a month) renders it unnecessary to record baselines during each analysis. Error calculations include the errors on mass discrimination measurement and the J value. ^{40}Ar, ^{39}Ar, ^{38}Ar, ^{37}Ar, and ^{36}Ar blanks were calculated before every new sample and after every three heating steps. ^{40}Ar blanks were between 6.5E-16 and 1.0E-15 moles. Blank values for m/e 39 to 36 were all less than 6.5E-17 moles. Age plateaus were determined using the criteria of Dalrymple and Lanphere (1974), and data reduction utilised ArArCalc (Koppers 2002). The samples were irradiated for 15 h (1 MW) in the OSU, CLICIT facility, and J values were calculated via the irradiation of Fish Canyon Tuff sanidines, which were separated by distances of <1 cm, throughout the columnar irradiation package.

Green hydrothermal biotite from the Divriği A-kafa orebody yield weighted mean plateau ages of 73.75± 0.62 Ma (2σ; TD 03040) and 74.34±0.83 Ma (2σ; TD 03041; Fig. 7, Table 3), which are indistinguishable. The two samples of brown hydrothermal biotite from the Hasançelebi prospect yield distinguishable plateau ages of 73.43±0.41 Ma (2σ; TH 03002) and 74.92±0.39 Ma (2σ; TH 03003), suggesting that two generations of brown hydrothermal biotite are present at Hasançelebi. The brown hydrothermal biotite (TH 03011) from a road cut south of the Hasançelebi prospect yields a weighted mean plateau age of 73.12±0.75 Ma (2σ; Fig. 7, Table 3).

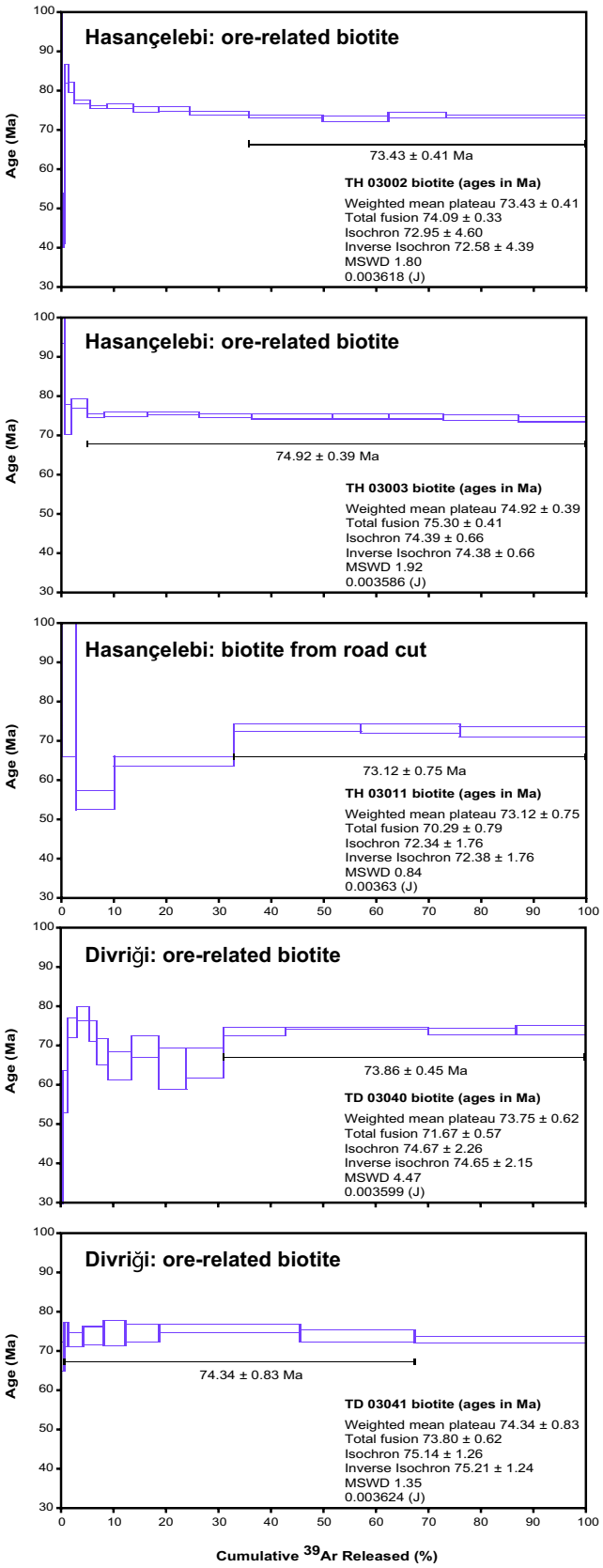

Fig. 7 $^{40}Ar/^{39}Ar$ age spectra of biotite

Stable isotope geochemistry

Sulfur isotope analysis

Sampling

Six pyrite samples have been prepared for sulfur isotope analysis (Table 2). Four of these are from the Divriği mine (TD 03033, TD 03040, TD 03042, TD 03049). Pyrite of sample TD 03033 has been extracted from a vein that contains two generations of calcite of which the earlier one hosts the pyrite and tourmaline needles. Pyrite of sample TD 03040 occurs disseminated and that of sample TD 03042 associated with calcite within the A-kafa massive magnetite ore. The pyrite of sample TD 03049 comes from a calcite–pyrite veinlet cutting the A-kafa magnetite body. Pyrite sample TH 03004 from Hasançelebi was extracted from a rock, which is mainly composed of diopside-scapolite with interstitial magnetite. The pyrite is cutting the altered rock and is, therefore, paragenetically late. Sample TK 03027 is from a drill core from the Karakuz mine (hole HS-2; Fig. 6b). The pyrite occurs interstitial to mushketovite, the pseudomorphic replacement of specular hematite by magnetite.

Analytical methods and results

The sulfur isotope analyses were carried out in the laboratories of the Université de Lausanne, Switzerland, and the TU Bergakademie Freiberg, Germany. In the facilities of the Institute of Mineralogy at Lausanne, sulfur isotope ratios are determined with an on-line elemental analyzer (EA) – continuous flow – isotope ratio mass spectrometer (IRMS). The EA–IRMS system consists of a Carlo Erba 1108 EA coupled by a continuous flow interface to the Finnigan Mat Delta S IRMS. The EA oxidizes all the sample compounds under a stream of helium and oxygen by flash combustion in a single oxidation-reduction quartz tube filled with oxidizing (tungsten trioxide) and reducing (elemental copper) agents at 1,030°C. Water was removed using anhydrous magnesium perchlorate, and the gases enter a chromatographic column (Poropak QS) for separation of SO_2, which is isotopically analyzed by IRMS (Giesemann et al. 1994). The reproducibility, assessed by replicate analyses of a laboratory standard (natural pyrite, working value=+6.1‰, synthetic barium sulfate, working value =+12.5‰ $\delta^{34}S$) was better than 0.2‰ (1σ).

At the stable isotope laboratory of the Institute of Mineralogy at Freiberg, the $\delta^{34}S$ analyses on sulfides were conducted after conversion to SO_2 in the presence of V_2O_5 and SiO_2 (Yanagisawa and Sakai 1983) on a Finnigan MAT Delta E mass spectrometer. For the measurements, an internal standard (SO_2) was used, which is calibrated against

Table 3 Results of $^{40}Ar/^{39}Ar$ analysis

Incremental heating step	Laser power (W)	$^{36}Ar(a)$	$^{37}Ar(ca)$	$^{38}Ar(cl)$	$^{39}Ar(k)$	$^{40}Ar(r)$	Age±2σ (Ma)	$^{40}Ar(r)$ (%)	$^{39}Ar(k)$ (%)	K/Ca±2σ
TD03002 biotite J value=0.003618										
1	2.70	0.00141	0.00041	0.00006	0.00215	0.02564	76.03±34.41	5.81	0.03	2.260±10.986
2	3.30	0.00197	0.00159	0.00010	0.01082	0.07923	47.18±6.97	11.99	0.15	2.934±3.358
3	3.75	0.00128	0.00180	0.00010	0.01397	0.10218	47.13±5.72	21.28	0.20	3.345±2.869
4	4.35	0.00686	0.00167	0.00025	0.04298	0.56782	84.23±2.35	21.88	0.61	11.086±8.970
5	4.80	0.00685	0.00274	0.00040	0.09301	1.17782	80.8±1.302	36.78	1.31	14.610±7.768
6	5.10	0.00498	0.00133	0.00063	0.21353	2.57088	76.92±0.43	63.59	3.01	68.993±46.653
7	5.55	0.00246	0.00254	0.00054	0.21992	2.60874	75.81±0.34	78.22	3.10	37.181±11.237
8	6.00	0.00380	0.00020	0.00094	0.36622	4.35422	75.98±0.36	79.49	5.16	796.072±3768.221
9	6.45	0.00182	0.00072	0.00094	0.33024	3.88223	75.15±0.52	87.81	4.65	197.651±315.024
10	7.05	0.00223	0.00335	0.00111	0.43649	5.13151	75.15±0.51	88.61	6.15	56.060±36.216
11	8.40	0.00345	0.01299	0.00245	0.79129	9.20883	74.41±0.46	90.03	11.14	26.198±12.671
12	9.90	0.00317	0.02486	0.00383	1.01705	11.68447	73.47±0.38	92.56	14.32	17.594±8.921
13	11.40	0.00304	0.05453	0.00415	0.87510	9.96291	72.82±0.59	91.71	12.32	6.901±2.406
14	13.50	0.00301	0.02325	0.00276	0.78353	9.03385	73.73±0.62	91.02	11.04	14.493±10.220
15	30.00	0.00575	0.05279	0.00692	1.90406	21.88811	73.51±0.35	92.78	26.82	15.509±7.826
	Σ	0.05209	0.18474	0.02519	7.10035	82.27843				
TH03003 biotite J value=0.003586										
1	4.20	0.00036	0.00048	0.00010	0.04439	0.51880	74.07±3.86	82.98	1.25	39.919±379.208
2	4.80	0.00086	0.00000	0.00000	0.10873	1.33886	77.96±1.20	84.00	3.05	0.000±0.000
3	5.40	0.00105	0.00327	0.00029	0.11847	1.40207	74.99±0.57	81.89	3.33	15.565±5.954
4	6.60	0.00176	0.00710	0.00066	0.28690	3.40666	75.23±0.47	86.77	8.06	17.376±3.368
5	7.80	0.00190	0.00115	0.00071	0.35738	4.25306	75.39±0.42	88.35	10.04	133.951±133.161
6	9.00	0.00112	0.00239	0.00073	0.35217	4.16310	74.90±0.43	92.60	9.89	63.372±25.968
7	10.50	0.00180	0.01235	0.00128	0.54925	6.48146	74.77±0.59	92.43	15.43	19.124±3.800
8	12.00	0.00145	0.03615	0.00090	0.38930	4.58992	74.71±0.66	91.45	10.94	4.630±0.356
9	13.50	0.00120	0.13708	0.00079	0.37617	4.43807	74.76±0.73	92.59	10.57	1.180±0.080
10	18.00	0.00191	0.04884	0.00114	0.50585	5.94114	74.43±0.62	91.32	14.21	4.454±0.437
11	30.00	0.00105	0.00185	0.00107	0.45585	5.33607	74.18±0.65	94.51	12.81	105.668±229.319
	Σ	0.01455	0.25066	0.00767	3.55907	42.20610				
TH03011 biotite J value=0.003630										
1	3.30	0.00063	0.00000	0.00000	0.02696	0.35129	83.38±17.38	65.41	2.62	0.000±0.000
2	3.90	0.00179	0.00235	0.00021	0.07520	0.64109	54.98±2.24	54.76	7.30	13.764±31.866
3	4.70	0.00473	0.01206	0.00063	0.23657	2.38775	64.92±1.22	63.08	22.96	8.432±4.520
4	5.40	0.00273	0.01550	0.00047	0.24766	2.83709	73.50±1.04	77.84	24.04	6.872±2.314
5	12.00	0.00085	0.01243	0.00072	0.19543	2.23022	73.23±1.31	89.88	18.97	6.760±3.449
6	30.00	0.00113	0.01850	0.00034	0.24778	2.79644	72.44±1.30	89.36	24.05	5.758±2.637
	Σ	0.01186	0.06084	0.00238	1.03026	11.27638				
TD03040 biotite J value=0.003599										
1	2.70	0.00114	0.00010	0.00004	0.00519	0.03730	46.08±28.25	9.94	0.05	22.013±841.999
2	3.30	0.00187	0.00293	0.00030	0.01718	0.08658	32.43±9.92	13.54	0.17	2.522±4.542
3	4.20	0.00508	0.02728	0.00175	0.08280	0.75330	58.12±5.31	33.39	0.84	1.305±0.817
4	6.60	0.00479	0.01157	0.00094	0.18927	2.21397	74.40±2.49	61.01	1.92	7.033±8.855
5	7.60	0.00548	0.00249	0.00010	0.21655	2.64999	77.75±1.67	62.08	2.19	37.369±104.394
6	6.45	0.00438	0.01203	0.00096	0.16772	1.93760	73.49±2.64	59.96	1.70	5.997±5.778
7	7.20	0.00355	0.04153	0.00274	0.20608	2.20420	68.14±3.40	67.74	2.09	2.134±1.374
8	8.70	0.00778	0.14890	0.00926	0.44005	4.45232	64.52±3.54	65.94	4.45	1.271±0.444
9	10.50	0.00825	0.08862	0.00610	0.50146	5.47407	69.52±2.74	69.19	5.08	2.433±1.590
10	12.90	0.01111	0.16422	0.01087	0.55139	5.52305	63.89±5.26	62.71	5.58	1.444±1.071
11	15.60	0.01475	0.19440	0.01318	0.69400	7.09471	65.18±3.87	61.94	7.02	1.535±1.038
12	18.00	0.01730	0.09730	0.00757	1.17588	13.53027	73.20±1.13	72.57	11.90	5.196±3.676
13	23.40	0.01755	0.08716	0.00880	2.70651	31.49274	74.01±0.30	85.85	27.39	13.352±7.073
14	26.40	0.01127	0.08632	0.00691	1.63461	18.80241	73.18±0.86	84.94	16.54	8.143±7.201
15	30.00	0.00890	0.06368	0.00546	1.29170	14.95170	73.63±1.14	85.03	13.07	8.722±9.216
	Σ	0.12322	1.02855	0.07497	9.88041	111.20422				

Table 3 (continued)

Incremental heating step	Laser power (W)	^{36}Ar(a)	^{37}Ar(ca)	^{38}Ar(cl)	^{39}Ar(k)	^{40}Ar(r)	Age±2σ (Ma)	^{40}Ar(r) (%)	^{39}Ar(k) (%)	K/Ca±2σ
TD03041 biotite J value=0.003535										
1	2.70	0.00268	0.00539	0.00020	0.01383	0.14763	68.48±3.75	15.74	0.47	1.103±0.242
2	3.30	0.00107	0.00600	0.00010	0.02118	0.24460	73.96±3.33	43.52	0.72	1.518±0.274
3	3.90	0.00270	0.05093	0.00047	0.08486	0.96346	72.74±1.82	54.66	2.90	0.717±0.056
4	4.50	0.00333	0.04003	0.00087	0.11159	1.28683	73.86±2.38	56.67	3.81	1.199±0.213
5	5.10	0.00393	0.04031	0.00155	0.11994	1.38945	74.19±3.23	54.49	4.09	1.279±0.388
6	5.70	0.00389	0.05534	0.00217	0.19715	2.29048	74.40±2.23	66.56	6.73	1.532±0.421
7	11.40	0.00662	0.06481	0.00477	0.77557	9.13273	75.39±1.06	82.34	26.46	5.145±2.910
8	15.00	0.00719	0.07939	0.00480	0.65165	7.49438	73.67±1.42	77.91	22.24	3.529±1.747
9	30.00	0.00827	0.12599	0.00513	0.95493	10.81704	72.58±0.78	81.56	32.58	3.259±0.987
	Σ	0.03969	0.46820	0.02006	2.93070	33.76659				

Standard deviation on all J values is 0.2% (1σ). All isotope data are corrected for blanks and mass discrimination, and ^{39}Ar and ^{37}Ar were corrected for post-irradiation radioactive decay. Steps that form the plateau are shown in bold type

the International Atomic Energy Agency standard NBS 127. The reproducibility was generally better than ±0.2‰. The sulfur isotope ratios are reported relative to the Vienna Canyon Diablo Troilite standard (V-CDT).

Pyrite from the iron deposits are consistently enriched in ^{34}S (Table 4). Sulfur isotope ratios of pyrite from the Divriği mine lie between 11.5 and 15.6‰ $\delta^{34}S_{CDT}$ and are slightly lower than the pyrite from the Karakuz mine (sample TK 03027; $\delta^{34}S_{(VCDT)}$=17.4‰) or from the Hasançelebi prospect (sample TH 03004; $\delta^{34}S_{(VCDT)}$=16.0‰).

Oxygen and carbon analysis and microthermometry

Sampling

Calcite from different locations, various host rock lithologies, and different paragenetic positions were analyzed for their oxygen and carbon isotope composition (Table 2). A composite vein with two generations of calcite has been sampled (sample TD 03033). The earlier calcite generation (TD 03033-I) is intergrown with tourmaline and pyrite ($\delta^{34}S_{(VCDT)}$=15.6 ‰), whereas the later generation (TD 03033-II) is from a monomineralic calcite vein. Sample TD 03049 is from a calcite–pyrite veinlet cutting the A-kafa massive magnetite (pyrite of this sample has $\delta^{34}S_{(VCDT)}$= 11.5‰). The calcite of sample TD 03035 cuts magnetite and is in turn cut by pyrite. This calcite also contains isolated flakes of green hydrothermal biotite. It is assumed that it is equivalent to the first generation calcite in sample TD 03033. Sample TD 03044 is from a barren calcite veinlet in the Murmano pluton. The calcite contains tourmaline, which appears to be paragenetically later than the calcite. Sample TD 03048 comes from a calcite veinlet in the serpentinite. The calcite veinlet shows internal colloform banding.

Table 4 Results of stable isotope analysis

Sample	Location	Material	δ^{13}C-VPDB (‰)	δ^{18}O-VSMOW (‰)	δ^{34}S-VCDT (‰)
TH 03004	Hasancelebi	Pyrite			16.0
TK 03027	Karakuz	Pyrite			17.4
TD 03033_1	Divriği	Calcite	−1.99	15.12	
TD 03033_2	Divriği	Calcite	2.00	18.71	
TD 03033	Divriği	Pyrite			15.6
TD 03035	Divriği	Calcite	−0.23	16.19	
TD 03040	Divriği	Pyrite			14.3
TD 03042	Divriği	Pyrite			13.4
TD 03044	Divriği	Calcite	−2.33	17.77	
TD 03048	Divriği	Calcite	−2.16	26.46	
TD 03049	Divriği	Calcite	−2.47	15.90	
TD 03049	Divriği	Pyrite			11.5

Analytical method and results

The stable isotope compositions of calcite were determined at the stable isotope laboratory of the GeoBioCenter, Munich, using an automated Thermo/Finnigan online preparation device "Gas Bench II" connected to a Thermo/Finnigan Delta plus IRMS using a continuous flow mode (Révész and Landwehr 2002). CO_2 was liberated from carbonate powders by reaction with phosphoric acid at 72°C under a helium (>99.996 vol%) atmosphere and collected in individual reaction tubes sealed with a septum. The isotopic compositions are reported as δ values in per mill relative to Vienna Standard Mean Ocean Water (V-SMOW) for oxygen and Vienna Peedee Belemnite (V-PDB) for carbon. Hydrothermal calcite yield $\delta^{18}O_{(VSMOW)}$ values between +15.1 and +26.5‰ and $\delta^{13}C_{(VPDB)}$ values between −2.5 and +2.0‰ (Table 2). Fluid inclusions have been

investigated at the Department of Earth and Environmental Sciences, Ludwig-Maximilians University Munich, using a Linkam THMSG 600 heating–freezing stage mounted on a modified Leitz Laborlux Pol 12 microscope. The stage was calibrated with synthetic standards, and reproducibility of measurements are ≤0.2°C.

Carbon and oxygen isotope fractionation between calcite and CO_2, HCO_3^-, or H_2O is strongly temperature-dependent, respectively. A meaningful interpretation of the stable isotope data requires information on the formation temperature of the calcite to calculate the isotopic composition of a fluid or dissolved carbon species in equilibrium. Unfortunately, suitable primary fluid inclusions in the calcite for an estimation of the formation temperature are scarce. Sample TD 03044 contains gas-rich (probably CO_2-bearing) inclusions, two-phase liquid-dominated inclusions with a vapor bubble (L–V), and hypersaline three-phase inclusions containing a halite crystal (L–V–S). The fluid inclusions are generally small, commonly <5 μm. The L–V and L–V–S inclusions homogenize mainly between 300 and 335°C, which represent minimum trapping temperatures for these fluids. Fluid inclusions in the other samples appear to be mainly of secondary origin. Calcite sample TD 03049 contains monophase liquid inclusion at room temperature and extremely scarce two-phase L–V inclusion with homogenization temperature (T_h) <86.5°C. Post-pyrite second-generation calcite (TD 03033_II) contains scarce two-phase L–V inclusion with a T_h of 115–122°C. Calcite sample TD 03048 is void of fluid inclusions visible under the microscope.

Discussion

Paragenetic relationships and spatial distribution of biotite, pyrite, and calcite suggest that they represent late alteration stages related to the magnetite formation at Divriği rather than a much younger, unrelated hydrothermal event. Similar relationships are found at Hasançelebi. Therefore, the geochronological or stable isotope data derived from biotite or pyrite and calcite, respectively, allow important conclusions regarding the time of the ore formation and the kind of fluids involved in the mineralization process.

All $^{40}Ar/^{39}Ar$ biotite weighted mean plateau ages, except one (sample TH 03003 with an age of 74.92±0.39 Ma), overlap within 2-sigma error (Fig. 8), suggesting that biotite alteration was regional-coeval during the Campanian (geologic time scale according to Gradstein et al. 2004). The biotite alteration ages also overlap with the cooling ages of the intrusion of the Murmano complex at Divriği (68 to 77 Ma; Boztuğ et al. 2007; Fig. 8). The $^{40}Ar/^{39}Ar$ weighted mean plateau ages of 73.75±0.62 and 74.34±0.83 Ma (TD 03040) yielded by green hydrothermal biotite that cuts the Divriği A-kafa represent minimum ages for the magnetite ore. Magnetite veins and ore-related alteration occur within the syenite–monzonite and monzonite porphyry, indicating that the intrusions predate mineralization. Therefore, the age of the felsic host rocks of the Murmano plutonic complex (Rb–Sr isochron age of 110±5 Ma at 1σ, Zeck and Ünlü 1988; K–Ar cooling ages from 76.6±0.6 to 77.2±1.8 Ma; Boztuğ et al. 2007) is the maximum age for the mineralization. If the interpretation is valid that the hydrothermal biotite belongs to the ore-related late alteration stages, the age of the mineralization should be similar to that of the biotite, i.e., about 74 Ma. The presence of green hydrothermal biotite intergrown with pyrite and flakes of green biotite occurring in pyrite-bearing calcite suggest that the pyrite and the calcite at Divriği also have an age of 74 Ma.

At the Hasançelebi prospect, at least parts of the magnetite are intergrown with brown hydrothermal biotite, and both magnetite ore and brown biotite probably formed roughly coeval (Fig. 6d, e). Therefore, the ages of brown

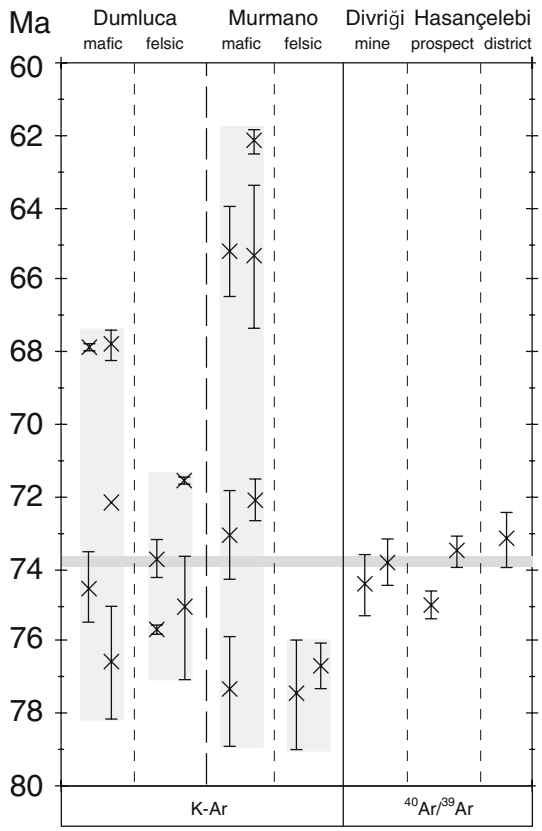

Fig. 8 Diagram showing minimum and maximum K–Ar cooling ages of magmatic biotite and/or amphibole of the Dumluca and Murmano plutonic complexes (Boztuğ et al. 2007) and the new $^{40}Ar/^{39}Ar$ weighted mean plateau ages of hydrothermal biotite. All but one of the $^{40}Ar/^{39}Ar$ ages overlap within their errors; therefore, these ages are indistinguishable. The data are compatible with the hypothesis that biotite alteration and iron mineralization occurred concomitantly with the cooling of postcollisonal plutons

biotite of 73.43±0.41 Ma (TH 03002) and 74.92±0.39 Ma (TH 03003) are interpreted to represent the ages for the epigenetic magnetite mineralization. However, these ages are distinctively different from each other, suggesting the presence of two generations of brown hydrothermal biotite. The dated biotite (TH 03011; 73.12±0.75 Ma) from a road cut south of the Hasançelebi iron prospect (Fig. 2) crosscuts the regional scale scapolite alteration affecting the volcanic rocks of the Deveci Volcanics and syenite porphyry dikes therein. Therefore, the field relationships imply that all ages reported here for the biotites from the Hasançelebi area (samples TH 03002, TH 03003, and TH 03011) constrain the minimum age of the volcanic host rocks (Deveci Volcanics), the porphyry dikes, and the scapolite alteration. Assuming that the Hasançelebi pluton, the volcanic rocks, and the altered syenite porphyry dikes are genetically related and that the scapolite alteration affecting this pluton (Yılmaz et al. 1993) is equivalent to that in the volcanic rocks and the porphyry dikes, these biotite ages also represent the minimum age of the Hasançelebi pluton.

The range of sulfur isotope composition of pyrite from Divriği, Karakuz, Hasançelebi between 11.5 and 17.4‰ $\delta^{34}S_{(VCDT)}$ is suggestive for a non-magmatic sulfur source. It lies within the range of sulfur isotope composition of Mesozoic seawater sulfate (Strauss 1997) and overlaps with $\delta^{34}S_{(VCDT)}$ values in the felsic host rocks of the Murmano pluton averaging 15.7‰.

The calcite samples from the Divriği deposit have relatively homogeneous $\delta^{18}O_{(VSMOV)}$ values between +15.1 and +18.7‰ and $\delta^{13}C_{(VPDB)}$ values between −2.5 and +2.0‰ if the sample taken from the serpentinite unit (TD 03048) with $\delta^{18}O_{(VSMOV)}$ value of +26.5‰ and a $\delta^{13}C_{(VPDB)}$ value of −2.2‰ is considered separately. This homogeneous stable isotope signature of all but one of the calcite samples, which let us assume that there are of the same origin, contrasts with the quite inhomogeneous fluid inclusion inventory. Most of the investigated multiple-phase fluid inclusions in calcite from Divriği homogenize between 115 and 335°C. These homogenization temperatures are similar to those of fluid inclusion in calcite from Hasançelebi reported by Sezerer-Kuru et al. (2006), which are between 80 and 320°C. If a calcite formation temperature of 300°C for all samples but TD 03048 is assumed, a fluid in equilibrium would have $\delta^{18}O_{(VSMOV)}$ values between +9.5 and +12.4‰ and $\delta^{13}C_{(VPDB)}$ values between −0.5 and +1.8‰ (fractionation factors for calcite-H_2O of Friedman and O'Neil 1977; for calcite-CO_2 of Ohmoto and Rye 1979). These data are consistent with the involvement of modified marine evaporitic fluids with carbon from seawater or from a marine limestone source. The calcite veinlet in serpentinite (TD 03048) shows internal colloform banding, which is suggestive for a lower formation temperature. If a temperature of 100°C is assumed, the calculated $\delta^{18}O_{(VSMOV)}$ values of an aqueous fluid would be 9.4‰ (fractionation factors for calcite-H_2O of Friedman and O'Neil 1977) and the $\delta^{13}C_{(VPDB)}$ values of −6.2‰ (fractionation factors for calcite-CO_2 of Ohmoto and Rye 1979) or −3.7‰ (fractionation factors for calcite-HCO_3^- of Deines et al. 1974), respectively. If this temperature estimate is valid, the oxygen isotope signature is similar to those of the other calcite samples. The $\delta^{13}C$ value is lower compared to the other samples. However, this carbon isotope signature is also compatible with a marine limestone source and could be caused by variation in the pressure, redox, and/or pH conditions. According to Ohmoto and Goldhaber (1997), the HCO_3^- produced by dissolution of carbonate probably has a similar $\delta^{13}C$ signature as the parent carbonate phase, and the $\delta^{13}C_{(VPDB)}$ value of −3.7‰ is at the lower end of the range of $\delta^{13}C$ values of marine carbonate or marble (e.g., Veizer and Hoefs 1976). CO_2 derived from thermal decarbonatization reactions is expected to have $\delta^{13}C$ values similar to that of the carbonate, i.e., at 0±4‰ if generated from normal limestone and −10±5‰ when generated from diagenetic carbonates (Ohmoto and Goldhaber 1997).

The stable isotope data on pyrite (and calcite) are suggestive for involvement of evaporite-derived fluids during the late mineralization stages. An involvement of evaporitic brines also during the early stages is compatible with the presence of the pre-magnetite Na–Ca scapolite alteration (Dipyre with 20–30 Mol% mejonite; Helke 1955) at Divriği and the large-scale, pervasive pre-magnetite scapolite alteration at Hasançelebi and Karakuz. Paleogeographic and paleoclimatic reconstructions are in agreement with such a hypothesis (see, e.g., Gürer 1994; Yildiz and Özdemir 1999; Yılmaz and Yılmaz 2006).

Field observations and data presented here are compatible with a model similar to that proposed by Stendal and Ünlü (1991) and Ünlü et al. (1995) in which brines with evaporitic components leach and redistribute iron from ophiolitic rocks concomitant with the cooling of the nearby plutonic rocks (e.g., Barton and Johnson 1996). However, a magmatic–hydrothermal contribution to the mineralization cannot be excluded based on the stable isotope data, and an alternative interpretation of these data is possible. The stable isotope signatures of plutonic rocks at Divriği may result from assimilation of crustal or evaporitic material, respectively (Boztuğ et al. 2007), and one can speculate whether hydrothermal fluids from these contaminated magmas could have formed the pyrite with the detected sulfur isotope composition. From our perspective, there are two points to consider: (1) assuming a similar genesis for Divriği, Karakuz, and Hasançelebi, the fact that the pyrite from all these deposits is enriched in ^{34}S would imply that, if this mineral precipitated from magmatic–hydrothermal fluids, the parent magmas at Karakuz and Hasançelebi would also be contaminated, and (2) the isotope values of the igneous rock

could also be produced by the interaction of evaporite-derived brines with the cooling plutons. The intrusions are affected by the hydrothermal alteration. In how far the alteration embraced the intrusions remains to be documented.

Conclusions

The new $^{40}Ar/^{39}Ar$ ages suggest that biotite alteration spatially related to magnetite mineralization at Divriği (74 Ma) and Hasançelebi (75 to 73) occurred roughly coeval in Campanian times. The age data are compatible with previously published Rb–Sr isochron (110 Ma) and K–Ar cooling ages (77 to 62 Ma) for the magnetite-bearing and hydrothermally altered plutons of the Murmano complex at Divriği. The biotite alteration temporally overlaps with the cooling of these plutons. The $^{40}Ar/^{39}Ar$ ages of biotite from Divriği represent minimum mineralization ages and imply that the ore formation of the Divriği A-kafa took place between 110 and 74 Ma, though we suggest that occurred close to 74 Ma. The ages of the biotite from the Hasançelebi ores are interpreted to represent mineralization ages based on magnetite–biotite intergrowth textures. These ages, together with the age from a biotite vein cutting the altered Deveci Volcanics, imply that the volcanic host rock, the syenite porphyry dikes therein, and the scapolite alteration affecting these rocks are Campanian or pre-Campanian in age. Sulfur isotope data suggest a non-magmatic sulfur source for the late-stage pyrite at Divriği, Hasançelebi, and Karakuz. These data (together with the stable isotopes of calcite from Divriği) are consistent with involvement of evaporite-derived fluids during late mineralization stages. The paleogeography, paleoclimate, pre-magnetite scapolitization, geochronologic, and stable isotope data presented permit that the magnetite ore formed mainly from evaporitic fluids though a magmatic–hydrothermal component to mineralization is not excluded.

Acknowledgments We are indebted to Zeynel Aslan and the management and employees of the Divriği and Karakuz mines for their support and hospitality. The geochronology laboratory at the University of Geneva is partly funded by the Swiss National Science Foundation. C. Mayr and U. Struck (GeoBioCenter, LMU) are thanked for oxygen and carbon isotope analysis. G. Janßen (LMU) performed photographs of handspecimens and thin sections, which is gratefully acknowledged. The manuscript benefited from valuable suggestions by F. Neubauer, H. Stendal, and B. Lehmann. We thank TUBITAK for travel grants to IK and RM.

References

Anonymous (2003) Maden tetkık ve arama genel müdürlügü Malatya ılı maden ve enerjı kaynaklari. MTA report. http://www.mta.gov.tr/madenler/Malatya.DOC

Ay Y, Yildirim S, Dumanlilar O, Turgut O, Tablaci A, Yildiz H, Dumanlilar H (2004) An example of Olympic Dam-type Fe oxide–Cu–Au–(Ag–Ba–F–U–Th–REE) deposits from Turkey: Hasançelebi Fe deposit. 57. Geological Congress of Turkey, Ankara, pp 107–108

Barton MD, Johnson DA (1996) Evaporitic source model for igneous related Fe oxide–(REE–Cu–Au–U) mineralization. Geology 24:259–262

Boztuğ D (1998) Post-collisional Central Anatolian alkaline plutonism, Turkey. Turk J Earth Sci 7:145–165

Boztuğ D, Harlavan Y (2007) K–Ar ages of granitoids unravel the stages of Neo-Tethyan convergence in the eastern Pontides and central Anatolia. Int J Earth Sci (in press) DOI 10.1007/s00531-007-0176-0

Boztuğ D, Harlavan Y, Arehart GB, Satır M, Avcı N (2007) K–Ar age, whole rock and isotope geochemistry of A-type granitoids in the Divriği-Sivas region, eastern–central Anatolia, Turkey. Lithos 97:193–218

Cihnioğlu M, Isbasarir O, Ceyhan U, Adiguzel O (1994) Iron inventory of Turkey (in Turkish). MTA, Ankara

Dalrymple GB, Lanphere MA (1974) $^{40}Ar/^{39}Ar$ age spectra for undisturbed terrestrial samples. Geochim Cosmochim Acta 38:715–738

Deines P, Langmuir D, Harmon RS (1974) Stable carbon isotope ratios and the existence of a gas phase in the evolution of carbonate ground waters. Geochim Cosmochim Acta 38:1147–1164

DPT (2001) Sekizinci Beş Yıllık Kalkınma Planı Madencilik ÖİK Raporu Metal. Madenler Alt Komisyonu Demir Çalışma Grubu Raporu (Commission for Mining Specialization; Metallic Ores Sub-commission, Iron study group report). Report no. 2624-ÖİK-635, ISBN 975-19-2864-8 pp 59. http://ekutup.dpt.gov.tr/madencil/metalmad/oik635.pdf

Friedman I, O'Neil JR (1977) Compilation of stable isotope fractionation factors of geochemical interest. In: Fleischer M (ed) Data of geochemistry. US Geological Survey Professional Paper 440-KK, p 12

Giesemann A, Jäger HJ, Normann AL, Krouse HR, Brand WA (1994) On-line sulfur-isotope determination using an elemental analyser coupled to a mass spectrometer. Anal Chem 66:2816–2819

Gradstein FM, Ogg JG, Smith AG, Bleeker W, Lourens LJ (2004) A new geologic time scale, with special reference to Precambrian and Neogene. Episodes 27:83–100

Gürer ÖF (1994) Hekimhan-Hasançelebi Yöresinin Üst Kretase Stratigrafisi ve Havza Evrimi. Geol Bull Turk 37:135–148

Gürer ÖF (1996) Geological position and the genesis of Hasançelebi alkaline magmatism at the eastern Taurides (NW Malatya). Turk J Earth Sci 5:71–88

Gumus A (1998) Endogenic ore deposits. Bilim Ofset, Izmir

Helke A (1955) Beobachtungen an türkischen Minerallagerstätten. Neues Jahrbuch für Mineralogie. Abhandlungen 88:55–224

Ilbeyli N, Pearce JA, Thirlwall MF, Mitchell JG (2004) Petrogenesis of collision-related plutonics in Central Anatolia, Turkey. Lithos 72:163–182

Isik MA (2005) Complex metasomatic process between serpentinized ultrabasic rocks and alkaline intrusive bodies in Divriği. EUG XI, Strassburg

Klemm DD (1960) Die Eisenerzvorkommen von Divrik (Anatolien) als Beispiel tektonisch angelegter pneumatolytisch-metasomatischer Lagerstättenbildung. Neues Jahrbuch für Mineralogie. Abhandlungen 94:591–607

Koppers AAP (2002) ArArCALC-software for $^{40}Ar/^{39}Ar$ age calculations. Comput Geosci 28:605–619

Kuşcu I, Gencalioglu-Kuscu G, Tosdal RM, Ullrich T, Friedman R (2007) Link between magmatism and subduction-related events in eastern–southeastern Turkey. Geophys Res Abstr 9:04814, 2007 SRef-ID: 1607-7962/gra/EGU2007-A-04814

Kuşcu I, Yılmazer E, Demirela G (2002) Sivas-Divriği Bölgesi Skarn Tipi Demir Oksit Yataklarına Fe-oksit-Cu-Au (Olympic Dam tipi) Perspektifinden Yeni Bir Bakıs. Geol Bull Turk 45(2):33–47

Kuşcu I, Yılmazer E, Demirela G, Gökçe H (2005a) Orta ve Batı Andalu'daki Bazı Skarn-Tipi" Fe-Oksit-Cu-Au (DOBA) Potansiyeli. Türkiye Demir Yataklari Jeolojisi, Madenciliği ve Mevcut Sorunları Sempozyumu Bildiriler Kitabı Hasiran Istanbaul 179–204

Kuşcu I, Yılmazer E, Demirela G, Gökçe H, Güleç N (2005b) Alteration zoning of iron oxide deposits in the Hasançelebi and Karakuz (Malatya) regions. 58. Turkish Geological Symposium, Ankara, pp 66–67 (in Turkish with English abstract)

Leo GW, Marvin RF, Mehnert HH (1973) Potassium–argon ages of igneous rocks in the Kulunçak-Sofular area, Malatya province, central Turkey. Internal MTA report, p 16

McDougall I, Harrison TM (1988) Geochronology and the thermochronology by the $^{40}Ar/^{39}Ar$ method. Oxford University Press, London

Özkoçak O (1970) Hasançelebi Skapolit - Manyetit Mineralizasyon Bölgesi. Madencilik IX 6:18–20

Öztürk H, Öztunali Ö (1993) Divriği demir yataklari üzerinde genç tektonizma etkileri ve sonuçları. Türkiye Jeoloji Kurumu Bülteni 8:97–106 (in Turkish with English abstract)

Ohmoto H, Goldhaber MB (1997) Sulfur and carbon isotopes In: Barnes HL (ed) Geochemistry of hydrothermal ore deposits, 3rd edn. Wiley, New York, pp 517–611

Ohmoto H, Rye RO (1979) Isotopes of sulfur and carbon. In: Barnes HL (ed) Geochemistry of hydrothermal ore deposits. Wiley, New York, pp 509–567

Parlak O, Yılmaz H, Boztuğ D (2006) Origin and tectonic significance of the metamorphic sole and isolated dykes of the Divriği ophiolite (Sivas, Turkey): evidence for slab break-off prior to ophiolite emplacement. Turk J Earth Sci 15:25–45

Révész KM, Landwehr JM (2002) $\delta^{13}C$ and $\delta^{18}O$ isotopic composition of $CaCO_3$ measured by continuous flow isotope ratio mass spectrometry: statistical evaluation and verification by application to Devils Hole DH-11 calcite. Rapid Commun. Mass Spectrom 16:2102–2114

Robertson AHF (2002) Overview of the genesis and emplacement of Mesozoic ophiolites in the eastern Mediterranean Tethyan region. Lithos 65:1–67

Şengör AMC, Yılmaz Y (1981) Tethyan evolution of Turkey: a plate tectonic approach. Tectonophysics 75:181–241

Sezerer-Kuru G, Kuşcu I, Şaliş B, Yılmazer E, Demirela G (2006) The formation conditions of iron oxide deposits in Hasançelebi (Malatya); a microthermometric approach. Miner Res Explor Bull 132:101–111 (in Turkish)

Stendal H, Ünlü T (1991) Rock geochemistry of an iron ore field in the Divriği region, Central Anatolia, Turkey: a new exploration model for iron ores in Turkey. J Geochem Explor 40:281–289

Stendal H, Ünlü T, Konnerup-Madsen J (1995) Geological setting of iron deposits of Hekimhan province, Malatya, central Anatolia, Turkey. Trans Inst Min Metall Sect B 104:B46–B54

Strauss H (1997) The isotopic composition of sedimentary sulfur through time. Paleogeogr Paleoclimatol Paleoecol 132:97–118

Tunc M, Ozcelik O, Tutkun Z, Gokce A (1991) Basic geological characteristics of the Divriği–Yakuplu–Ilic–Hamo (Sivas) area [in Turkish]. Doga. Turk J Eng Environ Sci 15:225–245

Uçurum A, Larson LT, Boztuğ D (1996) Geology, geochemistry, and petrology of the alkaline subvolcanic trachyte-hosted iron deposit in the Karakuz area, northwestern Hekimhan-Malatya, Turkey. Int Geol Rev 38:995–1005

Ünlü T, Stendal H, Makovicky E, Sayili S (1995) Genesis of the Divriği iron ore deposit, Sivas, central Anatolia, Turkey: an ore microscopy study. Bull Miner Res Explor Inst Turk 117:17–28

USGS (2007). Mineral yearbook 2005. http://minerals.usgs.gov/minerals/pubs/commodity/iron_&_steel/festemyb05.pdf

Veizer J, Hoefs J (1976) The nature of O^{18}/O^{16} and C^{13}/C^{12} secular trends in sedimentary carbonate rocks. Geochim Cosmochim Acta 40:1387–1395

Williams PJ, Barton MD, Johnson DA, Fontboté L, de Haller A, Mark G, Oliver NHS, Marschik R (2005) Iron oxide–copper–gold deposits: Geology, space-time distribution, and possible modes of origin. In: Hedenquist JW, Thompson JFH, Goldfarb RJ, Richards JP (eds) Economic Geology, 100th Anniversary Volume 1905–2005. Society of Economic Geologists, Littleton Colorado, pp 371–405.

Yalçin H, Gündoğdu MN, Gourgaud A, Vidal P, Uçurum A (1998) Geochemical characteristics of Yamadağı Volcanics in central east Anatolia: an example from collision-zone volcanism. J Volcanol Geotherm Res 85:303–326

Yanagisawa F, Sakai H (1983) Preparation of SO_2 for sulphur isotope ratio measurements by the thermal decomposition of $BaSO_4$–V_2O_5–SiO_2 mixtures. Anal Chem 55:985–987

Yigit O (2006) Gold in Turkey—a missing link in Tethyan metallogeny. Ore Geol Rev 28:147–179

Yildiz A, Özdemir Z (1999) Biostratigraphic and isotopic data on the Cöreklik Member of the Hekimhan Formation (Campanian–Maastrichtian) of SE Turkey and their palaeoenvironmental significance. Cretac Res 20:107–117

Yılmaz A, Yılmaz H (2006) Characteristic features and structural evolution of a post-collisional basin: the Sivas basin, Central Anatolia, Turkey. J Asian Earth Sci 27:164–176

Yılmaz H, Arikal T, Yılmaz A (2001) Günes ofiyolitinin jeolojisi. 54. Geological Congress of Turkey, Ankara, pp 54–65

Yılmaz S, Boztuğ D, Özturk A (1993) Geological setting, petrographic and geochemical characteristics of the Cretaceous and Tertiary igneous rocks in the Hekimhan–Hasançelebi area, northwest Malatya, Turkey. Geol J 28:383–398

Yılmazer E, Kuşcu I, Demirela G (2003) Divriği A-B Kafa Cevherlesmeleri: Alterasyon zonlanmasý ve zonlanma süreçleri. Geol Bull Turk 46:17–34

Zeck HP, Ünlü T (1988) Alpine ophiolite obduction before 110±5 Ma ago, Taurus belt, eastern Central Turkey—a preliminary note. Tectonophysics 145:55–62

Zeck HP, Ünlü T (1991) Shoshonitic, monzonitic pluton near Murmano, eastern Central Turkey—a preliminary note. Mineral Res Explor Bull 112:47–58